J. Fluid Mech. (1995), *vol.* 301, *pp.* 383–406

Double-diffusive convection with two stabilizing gradients: strange consequences of magnetic buoyancy

By D. W. HUGHES[1]† AND N. O. WEISS[2]

[1]Department of Mathematics and Statistics, University of Newcastle, Newcastle upon Tyne NE1 7RU, UK

[2]Department of Applied Mathematics and Theoretical Physics, University of Cambridge, Silver Street, Cambridge CB3 9EW, UK

(Received 17 June 1994 and in revised form 4 July 1995)

Instabilities due to a vertically stratified horizontal magnetic field (magnetic buoyancy instabilities) are believed to play a key role in the escape of the Sun's internal magnetic field and the formation of active regions and sunspots. In a star the magnetic diffusivity is much smaller than the thermal diffusivity and magnetic buoyancy instabilities are double-diffusive in character. We have studied the nonlinear development of these instabilities, in an idealized two-dimensional model, by exploiting a non-trivial transformation between the governing equations of magnetic buoyancy and those of classical thermosolutal convection. Our main result is extremely surprising. We have demonstrated the existence of finite-amplitude *steady* convection when *both* the influential gradients (magnetic *and* convective) are stabilizing. This strange behaviour is caused by the appearance of narrow magnetic boundary layers, which distort the mean pressure gradient so as to produce a convectively unstable stratification.

1. Introduction

One of the key problems in solar physics is to explain the means by which the Sun's interior magnetic field, which is predominantly azimuthal, escapes and subsequently emerges at the solar surface, thereby giving rise to sunspots and active regions. The most likely candidate for the initial disruption of the field is the instability mechanism known as magnetic buoyancy (see, for example, the reviews by Hughes & Proctor 1988; Hughes 1992), which is explained in detail below. The density of a magnetic gas is influenced both by the temperature and by the magnetic field, through the magnetic pressure. Both of these quantities diffuse and so the problem is of a double-diffusive nature. In their most natural form the equations are not those of classical double-diffusive convection; however, as shown by Spiegel & Weiss (1982), they can be made so by a suitable transformation. Thus magnetic buoyancy is another important double-diffusive process, joining many others that have been identified in a range of fields, including oceanography, geology, other astrophysical contexts and engineering (e.g. Huppert & Turner 1981). The most intensively studied double-diffusive system is thermosolutal (or thermohaline) convection, in which the fluid density depends

† Present address: Department of Applied Mathematical Studies, University of Leeds, Leeds LS2 9JT, UK.

on heat and solute concentrations; the ratio of the solutal to thermal diffusivities, denoted by $\tau = \kappa_s/\kappa$, typically is small ($\approx 1/80$ for salt in water). Recent numerical studies have revealed a wealth of fascinating nonlinear behaviour associated with this system (e.g. Moore & Weiss 1990).

Our aim in this paper is to study two-dimensional double-diffusive convection driven by magnetic buoyancy. We do this by investigating thermosolutal convection and exploiting the transformation of Spiegel & Weiss. It should be stressed that the identification of the two systems is not trivial; in thermosolutal convection the thermal and solutal gradients are, in some sense, independent, whereas, for magnetic buoyancy, variations in the magnetic field directly affect the temperature. Consequently, the physics of the magnetic system is more complicated than that of thermosolutal convection and is indeed somewhat surprising.

Putting aside diffusive considerations for the moment, the basic mechanism of the magnetic buoyancy instability of a stratified horizontal magnetic field is readily seen from a simple parcel argument (e.g. Acheson 1979). Suppose an atmosphere is in hydrostatic equilibrium with the pressure, density and magnetic field dependent only on height. Now suppose that a flux tube (or gas parcel) with magnetic field B, gas pressure p and density ρ is raised slowly, without bending, from a height z to a height $z + \mathrm{d}z$. Let 'δ' denote the changes in the internal properties of the tube and 'd' the changes in the external atmosphere.

Conservation of mass and magnetic flux of the tube leads to the relation

$$\frac{\delta B}{B} = \frac{\delta \rho}{\rho}, \tag{1.1}$$

and conservation of its specific entropy gives

$$\frac{\delta p}{p} = \gamma \frac{\delta \rho}{\rho}, \tag{1.2}$$

where $\gamma = c_p/c_v$ is the ratio of specific heats (for a perfect monatomic gas $\gamma = 5/3$). The tube will adjust rapidly to being in total pressure equilibrium with its surroundings; the magnetic pressure is given by $B^2/2\mu_0$ and so this leads to the relation

$$\delta p + \frac{B}{\mu_0}\delta B = \mathrm{d}p + \frac{B}{\mu_0}\mathrm{d}B. \tag{1.3}$$

The tube will continue to rise, showing the atmosphere to be unstable, if $\delta\rho < d\rho$. Manipulation of equations (1.1)–(1.3) thus leads to the following criterion for instability:

$$-M^2 \frac{\mathrm{d}}{\mathrm{d}z}\ln\left(\frac{B}{\rho}\right) > \frac{\mathrm{d}}{\mathrm{d}z}\ln\left(\frac{p}{\rho^\gamma}\right), \tag{1.4}$$

where $M^2 = B^2/\mu_0 p$ is the ratio of the square of the Alfvén speed ($B^2/\mu_0\rho$) to the square of the isothermal sound speed (p/ρ). The right-hand side describes the familiar convective stratification of the atmosphere; this is a stabilizing influence if $p\rho^{-\gamma}$ increases with height. The left-hand side reflects the influence of the magnetic field stratification, with stability if B/ρ increases upwards. In essence, a magnetic field that decreases upwards can support more of the atmosphere than would be possible in its absence, leading to a degree of top-heaviness.

Thus it is gradients of entropy $p\rho^{-\gamma}$ and B/ρ that affect the density, whereas the quantities that diffuse are the magnetic field B and the temperature T. The problem as it stands, therefore, is not in standard double-diffusive form; it can however be

made so by recognizing that the independent perturbation variables analogous to T and S (the solute concentration) in thermosolutal convection are, essentially, B and a special linear combination of B and T (Spiegel & Weiss 1982 and §2). This unusual choice of variables leads to some significant differences in the physics of the two systems.

The most interesting aspect in which they differ concerns the behaviour when both gradients are stabilizing. For thermosolutal convection, when $\mathrm{d}T/\mathrm{d}z > 0$ and $\mathrm{d}S/\mathrm{d}z < 0$, there are no instabilities of any kind, as one would expect; any perturbation to the static state will simply die away. However, if the ratio of magnetic to thermal diffusion (which we shall also denote by τ) is sufficiently small, then having $\mathrm{d}(p\rho^{-\gamma})/\mathrm{d}z > 0$ and $\mathrm{d}(B/\rho)/\mathrm{d}z > 0$ does not guarantee such straightforward behaviour for the magnetic system. Hughes (1985) demonstrated, by a linear analysis, the existence of oscillatory instabilities with two stabilizing gradients. The chief objective of this paper is to extend this work by investigating the nonlinear behaviour in this regime. Da Costa, Knobloch & Weiss (1981) performed a detailed analysis of the bifurcations and nonlinear solutions of thermosolutal convection by studying a fifth-order modal truncation of the governing equations; this system is quantitatively accurate to second order in amplitude and qualitatively accurate for larger amplitudes. On transforming to the magnetic problem, this truncated system predicts the surprising existence of a steady, sub-critical finite-amplitude solution when both gradients are stabilizing. This result can also be inferred from the analysis of Proctor (1981) who, by perturbation techniques, studied steady thermosolutal convection in the limit of very small τ. Our main concern has been to investigate in depth, by solution of the full nonlinear governing equations, the behaviour in the stable–stable regime. The key result of the paper is not simply to confirm that steady convection does indeed occur, even when both gradients are 'stabilizing', but, more importantly, to provide an explanation for the physical processes responsible. We are only concerned with the case when τ, the diffusivity ratio, is small; this is essential for the occurrence of the unusual behaviour outlined above and, furthermore, is the relevant astrophysical regime.

The layout of the paper is as follows. The governing equations and the relation between the magnetic and thermosolutal problems are described in §2. Section 3 contains a brief summary of the linear results; §4 describes the fifth-order system. The fully nonlinear solutions are discussed in §5, together with the physical explanation of this strange instability. Appendix A contains the detailed derivation of expressions (2.19) and (2.20) for B/ρ and $p\rho^{-\gamma}$. Appendix B considers briefly the effect of changing the lateral boundary conditions.

2. Mathematical formulation

The aim of this section is to formulate the governing equations of thermosolutal convection and magnetic buoyancy and to explain the relationship between the two systems. For thermosolutal convection we shall study the standard idealized model of two-dimensional convection in a horizontal layer confined between two planes, $z = 0$ (bottom) and $z = d$ (top). In the Boussinesq approximation the density is taken to be $\rho = \rho_0(1 - \tilde{\alpha}T + \tilde{\beta}S)$, where T is the temperature, S is the solute density and $\tilde{\alpha}, \tilde{\beta} > 0$ (throughout, a subscript 0 indicates a representative value). In equilibrium, when the fluid is at rest, T and S are given by

$$T = T_0 + \Delta T(1 - z/d), \qquad S = S_0 + \Delta S(1 - z/d). \tag{2.1}$$

If ΔT, ΔS are both positive, the layer is bottom-heavy and heated from below. For the perturbed state we introduce a stream function $\Psi(x,z)$ such that the velocity $\boldsymbol{u} = (-\partial_z \Psi, 0, \partial_x \Psi)$ and set

$$T = T_0 + \Delta T[1 - z/d + \Theta(x,z)], \quad S = S_0 + \Delta S[1 - z/d + \Sigma(x,z)]. \tag{2.2}$$

After scaling lengths with d and times with d^2/κ, where κ is the thermal diffusivity, the dimensionless governing equations can be written as

$$\partial_t \nabla^2 \Psi + J(\Psi, \nabla^2 \Psi) = \sigma R_a \partial_x \Theta - \sigma R_s \partial_x \Sigma + \sigma \nabla^4 \Psi, \tag{2.3}$$

$$\partial_t \Theta + J(\Psi, \Theta) = \partial_x \Psi + \nabla^2 \Theta, \tag{2.4}$$

$$\partial_t \Sigma + J(\Psi, \Sigma) = \partial_x \Psi + \tau \nabla^2 \Sigma. \tag{2.5}$$

Here

$$\sigma = \nu/\kappa, \quad \tau = \kappa_s/\kappa, \quad R_a = \frac{g\tilde{\alpha}\Delta T d^3}{\kappa\nu}, \quad R_s = \frac{g\tilde{\beta}\Delta S d^3}{\kappa\nu}, \tag{2.6}$$

where κ_s is the solutal diffusivity, ν is the kinematic viscosity, R_a and R_s are the thermal and solutal Rayleigh numbers. With this convention, R_a positive (negative) denotes a thermally unstable (stable) gradient; R_s positive (negative) is solutally stable (unstable). We restrict attention to the region $0 < x < \lambda$, $0 < z < 1$ and adopt the simplest boundary conditions, so that

$$\Psi = 0, \quad \partial_z^2 \Psi = 0, \quad \Theta = 0, \quad \Sigma = 0 \quad (z = 0, 1), \tag{2.7a}$$

$$\Psi = 0, \quad \partial_x^2 \Psi = 0, \quad \partial_x \Theta = 0, \quad \partial_x \Sigma = 0 \quad (x = 0, \lambda). \tag{2.7b}$$

For our investigations of magnetic buoyancy we consider perturbations to a static equilibrium state with a stratified horizontal magnetic field, $\boldsymbol{B} = B(z)\hat{\boldsymbol{y}}$. We employ a modified version of the Boussinesq approximation, as conceived by Spiegel & Weiss. The usual Boussinesq assumption holds concerning the smallness of the ratio of the layer depth to all scale heights; the difference is that it is not the perturbation in gas pressure that is assumed negligible, but rather the perturbation in the total pressure (gas + magnetic). As with the thermosolutal equations above, we shall restrict our attention to two-dimensional motions in the (x,z)-plane; such motions simply interchange magnetic field lines, which always remain in the y-direction. The description below of the governing equations is self-contained though brief; more details can be found in Spiegel & Weiss (1982). A formal derivation of the equations describing magnetic buoyancy in the Boussinesq approximation has been given by Corfield (1984).

Combining the magnetic induction equation with the continuity equation gives

$$\partial_t B + \boldsymbol{u} \cdot \nabla B + (\partial_x \Psi) B / H_\rho = \eta \nabla^2 B, \tag{2.8}$$

where $\boldsymbol{B} = B(x,z)\hat{\boldsymbol{y}}$, H_ρ is the density scale height and η is the magnetic diffusivity. Alternatively, this may be written as

$$\frac{\mathrm{D}\delta p_m}{\mathrm{D}t} + \alpha \partial_x \Psi = \eta \nabla^2 \delta p_m, \tag{2.9}$$

where δp_m is the perturbation in the magnetic pressure and $\alpha = (B_0^2/\mu_0)(\mathrm{d}/\mathrm{d}z)\ln(B/\rho)$, which is constant under the assumptions of the Boussinesq approximation.

Using the fact that $\delta p \approx -\delta p_m$, the energy equation can be written as

$$\frac{\mathrm{D}}{\mathrm{D}t}\left(\delta T + \frac{\delta p_m}{c_p \rho_0}\right) + \beta \partial_x \Psi = \kappa \nabla^2 \delta T, \tag{2.10}$$

where δT is the perturbation in temperature, c_p is the specific heat at constant pressure and $\beta = (T_0/\gamma)(\mathrm{d}/\mathrm{d}z)\ln(p\rho^{-\gamma})$ (constant, within the Boussinesq approximation). Equations (2.9) and (2.10) may be combined into standard advection–diffusion form:

$$\frac{\mathrm{D}\delta T^*}{\mathrm{D}t} + \beta^* \partial_x \Psi = \kappa \nabla^2 \delta T^*, \tag{2.11}$$

where

$$\beta^* = \beta - \frac{\alpha}{c_p \rho_0 (1-\tau)} \quad \text{and} \quad \delta T^* = \delta T - \frac{\tau \delta p_m}{c_p \rho_0 (1-\tau)}, \tag{2.12}$$

and where, for the magnetic problem, $\tau = \eta/\kappa$. On employing the usual scaling of lengths with d and times with d^2/κ, and defining Σ and Θ by

$$\delta p_m = -\Sigma \alpha d, \qquad \delta T^* = -\Theta \beta^* d, \tag{2.13}$$

equations (2.9) and (2.11) become (2.5) and (2.4) respectively.

Finally there is the momentum equation which, in the Boussinesq approximation, takes the form

$$\rho_0 \left(\partial_t \boldsymbol{u} + (\boldsymbol{u} \cdot \nabla)\boldsymbol{u} \right) = -g\rho \hat{\boldsymbol{z}} - \nabla \Pi + \rho_0 \nu \nabla^2 \boldsymbol{u}, \tag{2.14}$$

where $\Pi = p + p_m$ is the total pressure. Then the y-component of the curl of (2.14) is identical to equation (2.3) provided that we define

$$R_a = -\frac{g d^4 \beta^*}{\kappa \nu T_0}, \qquad R_s = \frac{g d^4 \alpha (\gamma - \tau)}{\kappa \nu p_0 \gamma (1-\tau)}. \tag{2.15}$$

Thus the governing equations of magnetic buoyancy can be transformed into those of thermosolutal convection and, at least in a formal sense, the systems may be regarded as being identical. However, this identification is made possible only by the introduction of somewhat unusual variables and Rayleigh numbers (particularly Θ and R_a) and, consequently, the physics of the two systems differs in some significant respects. In order fully to understand convection driven by magnetic buoyancy we must relate the natural variables and Rayleigh numbers to those defined by equations (2.13) and (2.15).

For magnetic buoyancy, the most natural Rayleigh numbers are defined by

$$R_t = -\frac{g \beta d^4}{\kappa \nu T_0}, \qquad R_b = \frac{g \alpha d^4}{\kappa \nu p_0}. \tag{2.16}$$

R_t, the natural analogue of R_a for thermosolutal convection, measures the degree of super- or sub-adiabaticity; $R_t < 0$ (> 0) implies convective stability (instability). R_b is a measure of the magnetic stratification; as shown in the introduction, $R_b > 0$ (< 0) denotes a magnetically stable (unstable) atmosphere. R_t and R_b are related to R_a and R_s, defined by (2.15), as follows:

$$R_s = \frac{(\gamma - \tau)}{\gamma(1-\tau)} R_b, \qquad R_a = R_t + \frac{(\gamma - 1)}{\gamma(1-\tau)} R_b. \tag{2.17}$$

The natural variables with which to describe magnetic buoyancy are the stream function Ψ (as in thermosolutal convection), δp_m and δT. In dimensionless form (after scaling pressure with $\kappa \nu p_0/gd^3$ and temperature with $\kappa \nu T_0/gd^3$) δp_m and δT are related to Θ and Σ as defined in (2.13) by

$$\delta p_m = -R_b \Sigma, \qquad \delta T - \frac{\tau(\gamma - 1)}{\gamma(1-\tau)} \delta p_m = \Theta \left(R_t + \frac{(\gamma - 1) R_b}{\gamma(1-\tau)} \right). \tag{2.18}$$

The transformations (2.17) and (2.18) are obviously singular when $\tau = 1$ and cannot be defined there; however, no problems arise in the limit as $\tau \to 1$. Although, for example, $O(1)$ values of R_t and R_b lead to very large values of $|R_a|$ and $|R_s|$, these are related by $R_a \approx R_s$ (from (2.17)). As we shall see in §3 (equations (3.2) and (3.3)) $R_a \approx R_s$ implies proximity to the stability boundary (when $\tau \to 1$) and hence Σ and Θ will indeed take $O(1)$ values, as expected for a problem with $O(1)$ values for R_t and R_b (but not obviously for one with very large values of $|R_a|$ and $|R_s|$).

The final step in the formulation of the problem is to specify the overall stratification, arising from the sum of the equilibrium state and the perturbations. This is more complicated than for thermosolutal convection where, given Θ and Σ, it is trivial to construct the total temperature and solute fields. Here the most economical description is in terms of B/ρ and $p\rho^{-\gamma}$; as described in detail in Appendix A these (dimensionless) fields are given by

$$B/\rho = \text{const.} + R_b(z - \Sigma) = \text{const.} + |R_b|\chi_b, \tag{2.19}$$

say;

$$p\rho^{-\gamma} = \text{const.} - \gamma R_t z + \left(\frac{1-\gamma}{1-\tau}\right) R_b \Sigma + \Theta\left(\gamma R_t + \frac{(\gamma-1)}{(1-\tau)} R_b\right) = \text{const.} + |R_t|\chi_p, \tag{2.20}$$

say. In our descriptions of the nonlinear evolution, in §5, we shall use the variables χ_b and χ_p to describe B/ρ and $p\rho^{-\gamma}$ respectively.

3. Linear theory

The linear theory of thermosolutal convection has been extensively studied (e.g. Turner 1973 and references therein). Linearization of the governing equations (2.3)–(2.5), followed by substitution of Fourier modes for Ψ, Θ and Σ, leads to the following cubic dispersion relation for the growth rate p:

$$p^3 + (1+\sigma+\tau)s^2 p^2 + [(\sigma+\tau+\sigma\tau)s^4 - (R_a - R_s)\sigma l^2/s^2]p + \sigma\tau s^6 + (R_s - \tau R_a)\sigma l^2 = 0, \tag{3.1}$$

where l and $n\pi$ (integer n) are the horizontal and vertical wavenumbers and $s^2 = l^2 + n^2\pi^2$. (The most unstable modes always have the simplest possible structure in the z-direction, i.e. $n = 1$.) The stability boundary for direct modes (when $p = 0$) is thus given by

$$R_a = R_a^{(e)} \equiv R_s/\tau + s^6/l^2, \tag{3.2}$$

and for oscillatory modes (at a Hopf bifurcation, when $p = \pm i\omega$ with ω real) by

$$R_a = R_a^{(o)} \equiv \left(\frac{\sigma+\tau}{\sigma+1}\right) R_s + (1+\tau)(1+\tau/\sigma)s^6/l^2, \tag{3.3}$$

provided that $\sigma(1-\tau)R_a > (\sigma+\tau)(s^6/l^2)$. The regions of linear stability and instability in the (R_a, R_s)-plane, together with the line of neutral buoyancy, are sketched in figure 1(*a*).

Using the transformation (2.17) the stability boundaries for the magnetic buoyancy problem become

$$R_t = R_t^{(e)} = R_b/\tau + s^6/l^2 \qquad \text{(direct modes)}; \tag{3.4}$$

$$R_t = R_t^{(o)} = \frac{(1+\tau+\sigma-\gamma)}{\gamma(1+\sigma)} R_b + \frac{(1+\tau)(\sigma+\tau)}{\sigma}\frac{s^6}{l^2} \qquad \text{(oscillatory modes)}. \tag{3.5}$$

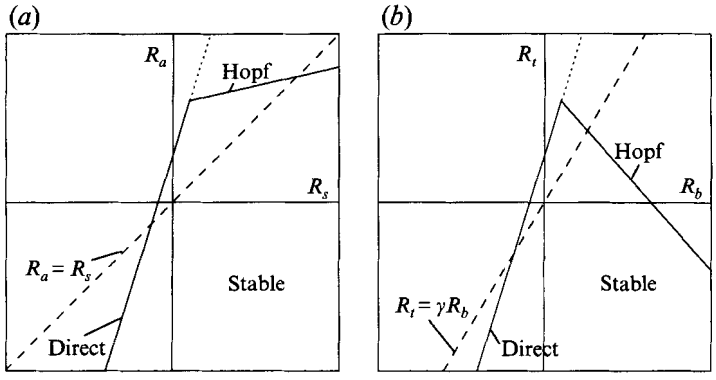

FIGURE 1. Sketches showing the regimes of linear stability in (*a*) the (R_s, R_a)-plane, and (*b*) the (R_b, R_t)-plane. The lines of direct and Hopf bifurcations are marked, together with the line of neutral buoyancy ($R_a = R_s$ in (*a*), $R_t = \gamma R_b$ in (*b*)).

The stability diagram, for the case of $\tau < \gamma - 1 - \sigma$, is sketched in figure 1(*b*). Also marked is the stability boundary in the absence of diffusion ($R_t = \gamma R_b$ from (1.4)); note that for this case the fourth quadrant ($R_t < 0$, $R_b > 0$) is stable.

Direct instability occurs primarily in the third quadrant ($R_t < 0, R_b < 0$) and, physically, is analogous to the salt-fingering instability of thermosolutal convection. When R_t and R_b are both negative the atmosphere is subadiabatically stratified and has B/ρ decreasing with height. The influence of the stabilizing temperature gradient on infinitesimal perturbations is diminished by the large thermal diffusivity, whereas the destabilizing magnetic field gradient is affected little by the weak magnetic diffusivity.

Oscillatory instability (overstability) can occur in both the first and fourth quadrants. When R_t and R_b are both positive (a superadiabatic atmosphere and B/ρ increasing with height) the instability mechanism is similar to that occurring in thermosolutal convection when R_a and R_s are both positive. The large thermal diffusivity lessens the destabilizing influence of the superadiabatic stratification whereas the small magnetic diffusion maintains the stabilizing magnetic gradient; consequently a fluid parcel (or flux tube) displaced upwards can find itself denser than its surroundings. The parcel thus falls, with diffusion causing it to return to its original level with a higher density than it had initially. It then overshoots below its equilibrium position, with repetition of this process leading to growing oscillations. As shown in figure 1(*b*), and as expected on physical grounds, if the atmosphere is sufficiently superadiabatic (R_t large enough) then a parcel displaced upwards will, despite the thermal diffusion and the stabilizing B/ρ gradient, find itself less dense than its surroundings and will continue to rise, i.e. there is a direct instability.

By far the most surprising feature of the magnetic problem is the appearance, for $\tau + \sigma < \gamma - 1 = 2/3$, of overstability in the fourth quadrant of the (R_t, R_b)-plane ($R_t < 0$, $R_b > 0$); i.e. instability with two stabilizing gradients (Hughes 1985). For this instability there is no simple analogy to be drawn with thermosolutal convection; there, as one would expect, no instability is possible when both the heat and solute gradients are stabilizing ($R_a < 0$, $R_s > 0$). The essential difference between the two systems is that whereas in thermosolutal convection the solutal and thermal fields are independent, for magnetic buoyancy the magnetic field has a direct influence on the temperature; indeed, as we have seen in §2, it is δp_m and the hybrid quantity δT^*, defined by (2.12), that are independent. The physical mechanism behind the instability

is again best explained by means of a parcel argument. In the absence of all diffusion a raised fluid parcel will be hotter than its surroundings if $(\gamma - 1)R_b + \gamma R_t > 0$ (see Hughes 1985). The parcel is of course denser than its surroundings (both gradients being stabilizing) and, with no diffusion, will oscillate about its equilibrium position. However, with finite thermal diffusion the parcel will transmit heat to its surroundings when displaced upwards; it will thus return to its original position cooler, and hence denser, than it was initially, and will overshoot. The process is then repeated, leading to growing oscillations. It is the aim of the following sections to explore the nonlinear behaviour in the regime where both gradients are stabilizing.

4. A fifth-order truncated model

We first construct a low-order model that allows us to study the relevant bifurcation structure analytically. For this purpose we begin with the thermosolutal problem, which has been investigated in some detail (Da Costa *et al.* 1981). It is convenient to introduce the scaled quantities

$$\varpi = \frac{4\pi^2}{s^2}, \quad t^* = s^2 t, \quad r_a = \frac{l^2}{s^6} R_a, \quad r_s = \frac{l^2}{s^6} R_s. \tag{4.1}$$

Then we adopt a minimal Fourier representation of the variables, so that

$$\Psi = 2^{3/2}\left(\frac{s}{l}\right) \sin lx \sin \pi z \, a(t^*), \tag{4.2}$$

$$\Theta = \frac{2^{3/2}}{s} \cos lx \sin \pi z \, b(t^*) - \frac{1}{\pi} \sin 2\pi z \, c(t^*), \tag{4.3}$$

$$\Sigma = \frac{2^{3/2}}{s} \cos lx \sin \pi z \, d(t^*) - \frac{1}{\pi} \sin 2\pi z \, e(t^*), \tag{4.4}$$

and obtain the truncated fifth-order system

$$\dot{a} = \sigma[-a + r_a b - r_s d], \tag{4.5}$$

$$\dot{b} = -b + a(1 - c), \tag{4.6}$$

$$\dot{c} = \varpi(-c + ab), \tag{4.7}$$

$$\dot{d} = -\tau d + a(1 - e), \tag{4.8}$$

$$\dot{e} = \varpi(-\tau e + ad), \tag{4.9}$$

where the dots indicate differentiation with respect to t^* (Veronis 1965; Da Costa *et al.* 1981).

The stability of the trivial solution $a = b = c = d = e = 0$ has already been discussed. The system possesses a symmetry $(a, b, d) \to (-a, -b, -d)$, $(c, e) \to (c, e)$, so direct modes set in at a pitchfork bifurcation when $r_a = r_a^{(e)}$, while oscillatory modes set in at a Hopf bifurcation when $r_a = r_a^{(o)}$, where

$$r_a^{(e)} = 1 + \frac{r_s}{\tau}, \qquad r_a^{(o)} = 1 + (1 + \sigma + \tau)\frac{\tau}{\sigma} + \left(\frac{\sigma + \tau}{\sigma + 1}\right) r_s, \tag{4.10}$$

from (3.2) and (3.3). The system (4.5)–(4.9) possesses a non-trivial steady solution satisfying the relationship

$$r_a = (1 + a^2)\left(1 + \frac{\tau r_s}{\tau^2 + a^2}\right). \tag{4.11}$$

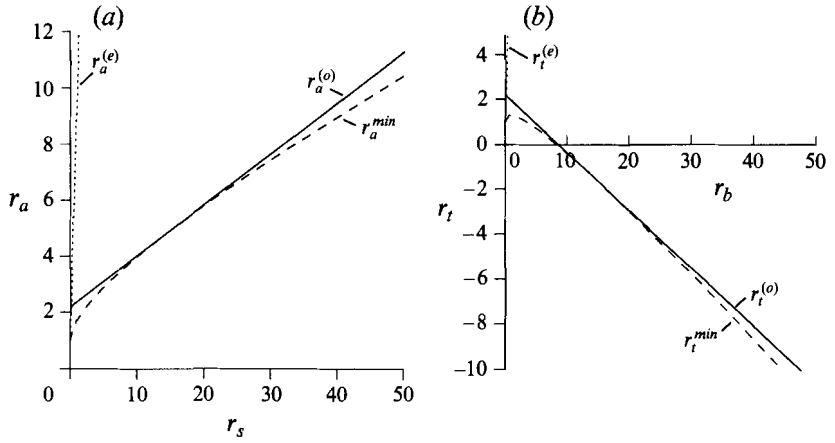

FIGURE 2. Bifurcations in the fifth-order model system with $\sigma = \tau = 0.1$. (*a*) The thermosolutal problem: in the (r_s, r_a)-plane, pitchfork bifurcations (at $r_a^{(e)}$) are marked by a dotted line, Hopf bifurcations (at $r_a^{(o)}$) by a full line, while the broken line corresponds to $r_a^{\min}$. (*b*) The magnetic buoyancy problem, showing the (r_b, r_t)-plane. Note the existence of both steady and oscillatory solutions with $r_t < 0$. In both plots the direct bifurcation lines lie very close to the vertical axis and so are only just visible.

Near the pitchfork bifurcation at $r_a^{(e)}$ we therefore have

$$r_a = \left(1 + \frac{r_s}{\tau}\right) + \left[1 - \frac{(1-\tau^2)}{\tau^3} r_s\right] a^2 + O(a^4), \tag{4.12}$$

and there are subcritical steady solutions (with $r_a < r_a^{(e)}$) provided $r_s > \tau^3/(1-\tau^2)$. In that case there is a turning point (corresponding to a saddle-node bifurcation) on the steady branch at $r_a = r_a^{min}$, where

$$r_a^{min} = [(1-\tau^2)^{1/2} + (\tau r_s)^{1/2}]^2 . \tag{4.13}$$

Now for $r_a > 0$ the Hopf bifurcation only occurs if $\tau < 1$ and $r_s > \tau^2(1+\sigma)/\sigma(1-\tau) > \tau^3/(1-\tau^2)$. So there are always subcritical steady solutions if there is an oscillatory bifurcation. Moreover, it can be shown that $1 < r_a^{min} \leqslant r_a^{(o)}$, that $r_a^{min} = r_a^{(o)}$ when $r_s = [(1+\sigma)^2\tau(1+\tau)]/[\sigma^2(1-\tau)]$, and that

$$r_a^{min} \sim \tau(\sigma+1) r_a^{(o)}/(\sigma+\tau) \quad \text{as } r_a \to \infty . \tag{4.14}$$

Figure 2(*a*) shows the location of the bifurcations at $r_a^{(e)}$, $r_a^{(o)}$ and r_a^{min} in the (r_s, r_a)-plane. The Hopf bifurcation at $r_a^{(o)}$ is supercritical unless r_s is fairly large, and the oscillatory branch terminates in a heteroclinic bifurcation (at $r_a^{(h)}$) on the unstable portion of the steady branch, as indicated in the schematic bifurcation diagram in figure 3(*a*).

These results can be translated to describe magnetic buoyancy. As in equation (2.17), we set

$$r_t = r_a - (\gamma - 1) r_s/(\gamma - \tau), \qquad r_b = \gamma(1-\tau) r_s/(\gamma - \tau), \tag{4.15}$$

and we assume that $(\sigma + \tau) < (\gamma - 1)$. Then there is a pitchfork bifurcation at $r_t = r_t^{(e)}$ and a Hopf bifurcation at $r_t = r_t^{(o)}$. Once again, there are subcritical steady solutions,

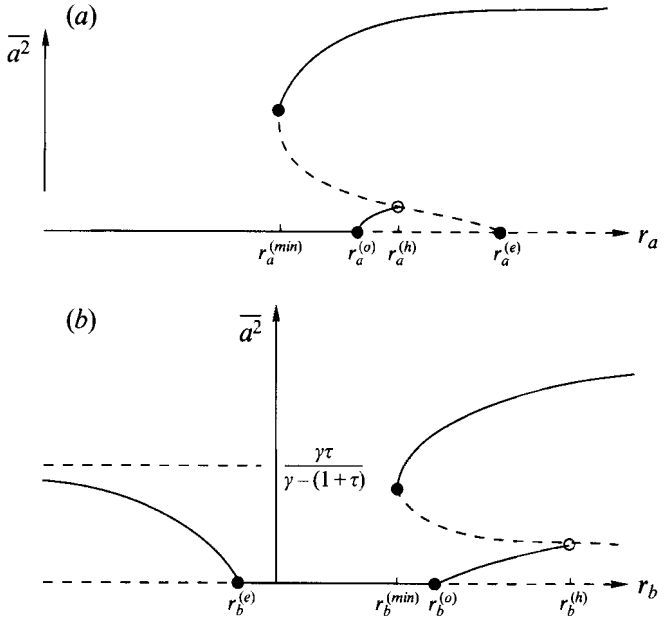

FIGURE 3. Bifurcation diagrams for the fifth-order model system: sketches showing $\overline{a^2}$, the mean square value of a, for steady and periodic solutions. (*a*) Behaviour as r_a is increased for fixed $r_s > \tau^2(1+\sigma)/\sigma(1-\tau)$. (*b*) The same, but as r_b is increased for a fixed *negative* value of r_t. The pitchfork bifurcation occurs for $r_b < 0$. Filled (open) circles denote local (global) bifurcations.

provided that $r_b > \gamma\tau^3/(\gamma-\tau)(1+\tau)$, with a turning point at

$$r_t^{min} = \left[(1-\tau^2)^{1/2} + \left\{\frac{\tau(\gamma-\tau)}{\gamma(1-\tau)} r_b\right\}^{1/2}\right]^2 - \frac{\gamma-1}{\gamma(1-\tau)} r_b. \tag{4.16}$$

Thus r_t^{min} is negative for r_b sufficiently large, and

$$r_t^{min} \sim -\frac{\gamma-(1+\tau)}{\gamma} r_b \quad \text{as } r_b \to \infty. \tag{4.17}$$

Moreover, $r_t^{min} \leqslant r_t^{(o)}$, so the bifurcation set is as shown in figure 2(*b*) and there are both steady and oscillatory nonlinear solutions in the quadrant where there are two stabilizing gradients.

Near the codimension-two point at $r_b = \gamma\tau^2(1+\sigma)/\sigma(\gamma-\tau), r_t = 1+\gamma\tau(1+\sigma)/\sigma(\gamma-\tau)$, where $r_t^{(e)} = r_t^{(o)}$, the bifurcation structure as r_t is increased for fixed r_b is similar to that shown in figure 3(*a*). For r_b sufficiently large, both the turning point and the Hopf bifurcation take place with $r_t < 0$, while the pitchfork bifurcation follows much later with $r_t \sim r_b/\tau$. Figure 3(*b*) shows the bifurcation structure for the model system when r_b is varied for fixed $r_t < 0$. There is no stationary bifurcation with $r_b > 0$ but for r_b large and positive there are two steady solutions, one stable and the other unstable. These solutions merge in a saddle-node bifurcation at the turning point, while the oscillatory solutions die in a heteroclinic bifurcation. For $r_b < 0$ there is another steady branch (in the 'salt-fingering' regime) with an amplitude that tends to an asymptotic value $a^2 \sim \gamma\tau/(\gamma-1-\tau)$ as $r_b \to -\infty$.

This truncated model suggests that subcritical steady convection does indeed occur when $R_t < 0$ and $R_b > 0$, contrary to naive expectations. Furthermore, the steady

solutions have much greater amplitudes than those on the short oscillatory branch. It is known, however, from comparisons between solutions of equations (4.5)–(4.9) and those obtained by numerical integration of the full partial differential equations, that the fifth-order system exaggerates the extent of subcriticality. So we have to solve the full problem.

5. Steady convection with two stabilizing gradients

5.1. *Subcritical convection at small* τ

The fifth-order system of ordinary differential equations discussed in §4 provides a good qualitative guide to the nonlinear behaviour of the partial differential equations (2.3)–(2.5); however, away from the immediate neighbourhood of bifurcation points it is not quantitatively accurate. Thus, although we can be sure that steady convection occurs for $R_a < R_a^{(e)}$, we cannot infer the value of R_a^{min}. Indeed, as stated above, it is well known that the fifth-order system exaggerates subcritical behaviour for thermosolutal convection; for the full partial differential equations R_a^{min} is always found to exceed $R_a^{(o)}$. The key question is whether R_a^{min} is sufficiently small that, after translation into the magnetic problem, steady convection can occur with $R_t < 0$, $R_b > 0$ and, if so, why? To provide an answer we need to solve the full governing equations (2.3)–(2.5). We use a numerical code kindly supplied by Dr D.R. Moore, which is identical with that described by Moore, Weiss & Wilkins (1991). To facilitate the computation, all solutions are constrained to be point-symmetric, but this restriction does not affect the issues that concern us here. Although there have been several detailed numerical investigations of thermosolutal convection, none of them are of direct relevance to the present problem. From the analysis of §§3,4 we know that the unusual behaviour we are seeking certainly requires $\sigma + \tau < \gamma - 1$, whereas in numerical simulations of thermosolutal convection it has however been customary to take $\sigma = 1$, thus violating this inequality. The results to be presented here go beyond those of Huppert & Moore (1976) in using smaller values of σ and τ and also in pinning down the dependence of R_a^{min} on R_s.

Guided by the fifth-order system, which suggests the existence of strange behaviour for $\sigma + \tau < \gamma - 1 = 2/3$, we decided, initially, to take $\tau = \sigma = 0.1$. The aspect ratio of the computational domain was taken to be 1.5, with $N_x = 96$ grid points in the horizontal direction and $N_z = 64$ points in the vertical (though the assumption of point-symmetry means that only half of these are used). Identifying the location of the turning point at the onset of steady convection is a lengthy though straightforward numerical procedure, accomplished by following the steady branch as R_b is decreased at fixed R_t; R_b is decreased in steps of magnitude I, where I depends on the value of R_b (see the caption to table 1). For $\tau = \sigma = 0.1$ the turning point is always located in the first quadrant of the (R_b,R_t)-plane ($R_b, R_t > 0$) and thus for these values of the diffusivity ratios there is no steady convection in the fourth quadrant. The values of R_t and R_b (also R_a and R_s) at the turning point are contained in table 1. As global measures of the nonlinear behaviour, table 1 also contains the values of the thermal and solutal Nusselt numbers, defined by

$$N_a = 1 - \lambda^{-1} \int_0^\lambda \partial_z \Theta(x,0)\mathrm{d}x, \qquad N_s = 1 - \lambda^{-1} \int_0^\lambda \partial_z \Sigma(x,0)\mathrm{d}x\,; \tag{5.1}$$

N_s is seen to exceed N_a considerably. In figure 4 the turning point values are plotted in both the (R_s, R_a)- and (R_b, R_t)-planes, together with the linear stability boundaries

R_t	R_b	R_a	R_s	N_a	N_s
1000	330°	1147	345	1.46	4.83
2000	3100†	3378	3238	2.24	6.78
3000	6500†	5889	6789	2.66	7.94
4000	10400†	8622	10862	2.98	8.87
5000	14500‡	11444	15144	3.42	10.25
6000	19500‡	14667	20367	3.65	10.95
7000	25000*	18111	26111	3.86	11.56
8000	30000*	21333	31333	4.24	12.78
9000	37000*	25444	38644	4.35	13.05
10000	43000*	29111	44911	4.65	13.99

TABLE 1. Values of R_t, R_b (equivalently R_a, R_s) at the end of the steady branch, together with the Nusselt numbers N_a and N_s; $\tau = 0.1$, $\sigma = 0.1$. For a fixed R_t, R_b is decreased in steps of I until no steady solution is found, where $I = 10(\diamond)$, $I = 100(\dagger)$, $I = 500(\ddagger)$, $I = 1000(*)$.

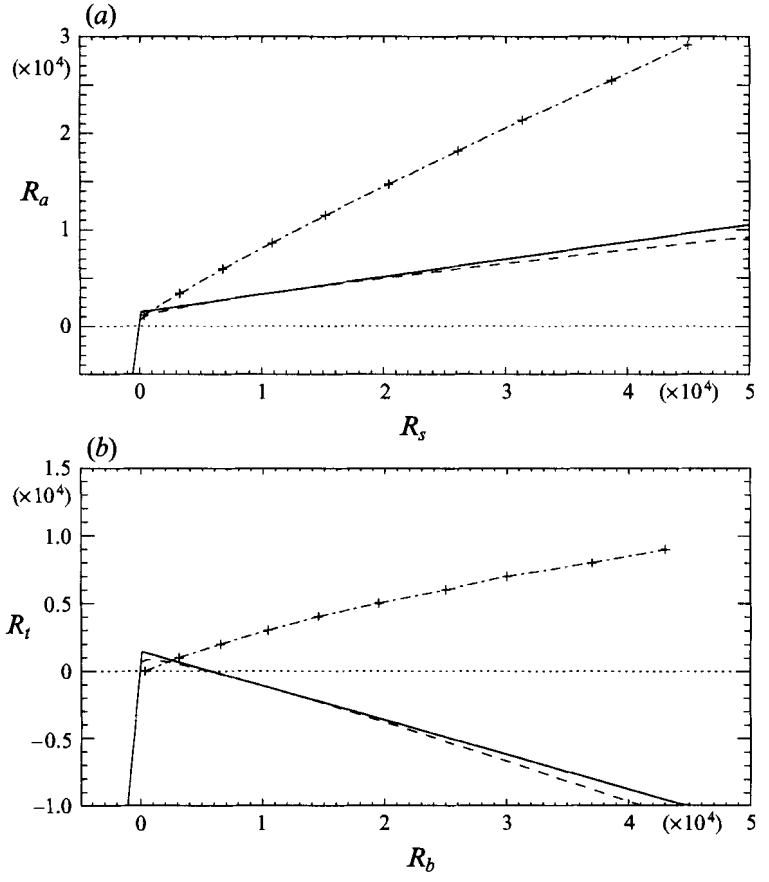

FIGURE 4. (*a*) Important regimes in the (R_s, R_a)-plane delineated for the case of $\sigma = 0.1$, $\tau = 0.1$. The solid lines show the linear stability boundary; the dotted line denotes $R_a = 0$; the dashed line is the prediction of R_a^{min} from the fifth-order system; the crosses (joined by a dash-dotted line) are the values of R_a^{min} calculated from the full PDEs. (*b*) As in (*a*), but for the (R_b, R_t)-plane. Note that R_t^{min} calculated from the full PDEs is always positive.

R_t	R_b	R_a	R_s	N_a	N_s
0	9000	11777	29177	3.92	29.86
-1000	40000	15244	40244	4.25	32.31
-2000	50000	18305	50305	4.54	34.53
-3000	59000	20959	59359	4.72	35.89
-4000	68000	23614	68414	4.95	37.65
-5000	76000	25863	76463	5.07	38.45
-6000	84000	28112	84512	5.15	38.99

TABLE 2. Values of R_t, R_b (equivalently R_a, R_s) at the end of the steady branch, together with the Nusselt numbers N_a and N_s; $\tau = 0.015$, $\sigma = 0.1$. For a fixed R_t, R_b is decreased in steps of 1000 until no steady solution is found.

and the prediction of R_a^{min} (R_t^{min}) from the fifth-order system. It is seen that R_a^{min} (R_t^{min}) comfortably exceeds $R_a^{(o)}$ ($R_t^{(o)}$) — and hence, of course, R_a^{min} (R_t^{min}) from the fifth-order system.

The result (4.13) shows clearly that, for the fifth-order system at least, R_a^{min} is minimized as $\tau \to 0$; thus we reduced the value of τ to $\tau = 0.015$, still with $\sigma = 0.1$. Reducing τ leads to a reduction in the thickness of the solutal boundary layers, and hence ensuring resolution of the boundary layers requires an increase in the number of grid points; we were confident of our results only for the high resolution of $N_x = 192$, $N_z = 128$. The convergence of such runs to a steady state, even starting from a nearby steady state, is painfully slow, and hence evaluation of R_t^{min} is an incredibly long-winded business; I, the step-size for decreasing R_b is taken to be 1000. The good news though is that with this reduced value of the magnetic diffusivity, steady convection does indeed extend into the stable–stable quadrant of the (R_b, R_t)-plane. The values of R_t and R_b at the turning point are contained in table 2 and are also plotted in figure 5; just as when $\tau = 0.1$ (figure 4) R_t^{min} (R_a^{min}) exceeds $R_t^{(o)}$ ($R_a^{(o)}$).

Contour plots of Ψ, the voriticity ω, T and S for the steady solution with $R_b = 50000$, $R_t = -2000$ ($R_a = 18305$, $R_s = 50305$) are shown in figure 6. In addition we show in figure 6(*e*) the normalized density field

$$\rho = R_s S - R_a T. \tag{5.2}$$

Solid (dotted) contours indicate positive (negative) values and the zero contour is dashed. At the bottom boundary ($z = 0$), $\rho = -\frac{1}{2}(R_a - R_s)$ while at the top boundary ($z = 1$), $\rho = \frac{1}{2}(R_a - R_s)$. Thus the basic density stratification is stabilizing ($\mathrm{d}\rho/\mathrm{d}z < 0$) for the values of R_a and R_s considered here. The domain is occupied by a single eddy rotating clockwise. Boundary layers form for both the thermal and solutal fields with the solutal boundary layers $O(\tau^{1/2})$ thinner than those of the temperature field. These are seen clearly in figure 7, which shows the horizontally averaged temperature and salinity distributions as functions of height. (The central region has an almost uniform solute concentration ($S \approx 0$) and so in figure 6(*d*) we have chosen not to plot the zero contour.) The density field, given by (5.2), has a more complicated structure than either T or S. Despite the fact that the density stratification is bottom-heavy, the double-diffusive processes lead to plumes of rising light fluid and falling heavy fluid. The consequent variation of ρ with x generates vorticity with the spatial structure shown in figure 6(*b*).

It is easy to see why subcritical steady solutions appear in the thermosolutal problem when $\tau \ll 1$. If vigorous motion is established, the stabilizing solutal stratification

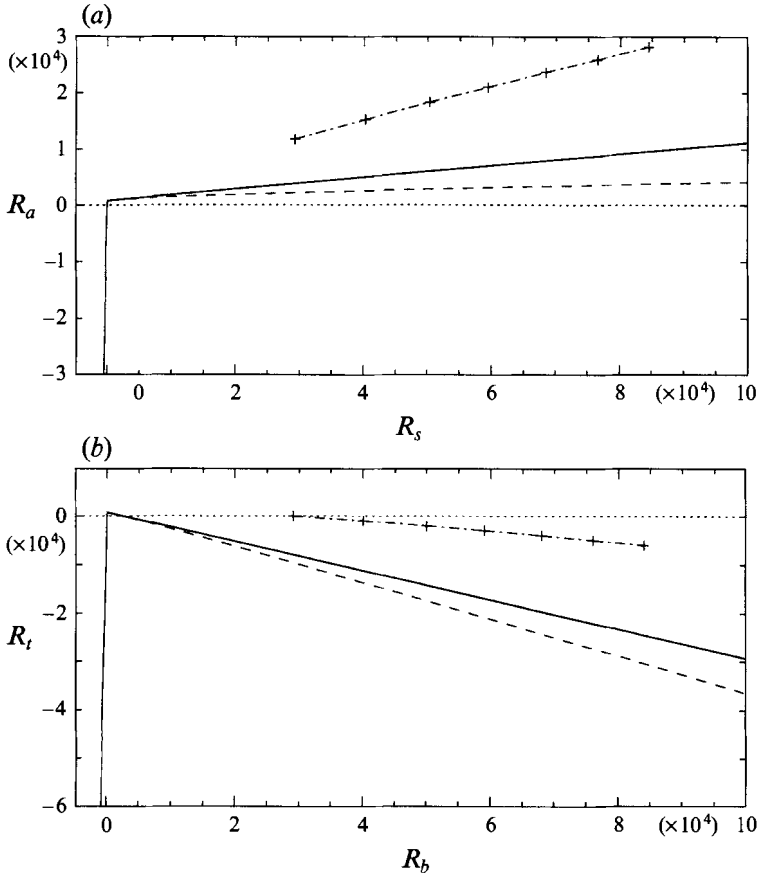

FIGURE 5. (*a*) As figure 4(*a*), but with $\tau = 0.015$. (*b*) As in (*a*), but for the (R_b, R_t)-plane. Note that R_t^{min} calculated from the full PDEs is now negative.

will be confined to narrow boundary layers of thickness $\delta_s \approx (\tau/U)^{1/2}$, where U is a typical dimensionless velocity, leaving the bulk of the fluid free for convection to be driven by the supercritical thermal gradient. This argument can be made more precise if we suppose that $\sigma \gg 1$, so that the Reynolds number is small. Then the equation of motion can be linearized and the velocity split into two components, driven by solute and heat respectively (cf. Galloway, Proctor & Weiss 1978). We suppose that these components are driven by narrow solutal and thermal plumes, with a core of uniform vorticity. Thus we set $\boldsymbol{u} = \boldsymbol{u}_s + \boldsymbol{u}_t$ and consider the vorticities $\boldsymbol{\omega}_s = \nabla \times \boldsymbol{u}_s$ and $\boldsymbol{\omega}_t = \nabla \times \boldsymbol{u}_t$. To estimate these we need only consider a one-dimensional problem with

$$\frac{\partial^2 \omega_s}{\partial x^2} = R_s \frac{\partial \Sigma}{\partial x} \tag{5.3}$$

and plumes of thickness δ_s. It follows that $\omega_s \approx -R_s \delta_s$ and, similarly, that $\omega_t \approx R_a \delta_t$, where δ_t is the thickness of the thermal plumes (Galloway *et al.* 1978). For convection to occur we require that $||\boldsymbol{u}_t|| > ||\boldsymbol{u}_s||$, with some suitably defined norm, so that $R_a \gtrsim (\delta_s/\delta_t) R_s$; but $(\delta_s/\delta_t) \approx \tau^{1/2}$, so we expect to obtain nonlinear solutions if $R_a > R_a^{min}$, where

$$R_a^{min} \approx \tau^{1/2} R_s. \tag{5.4}$$

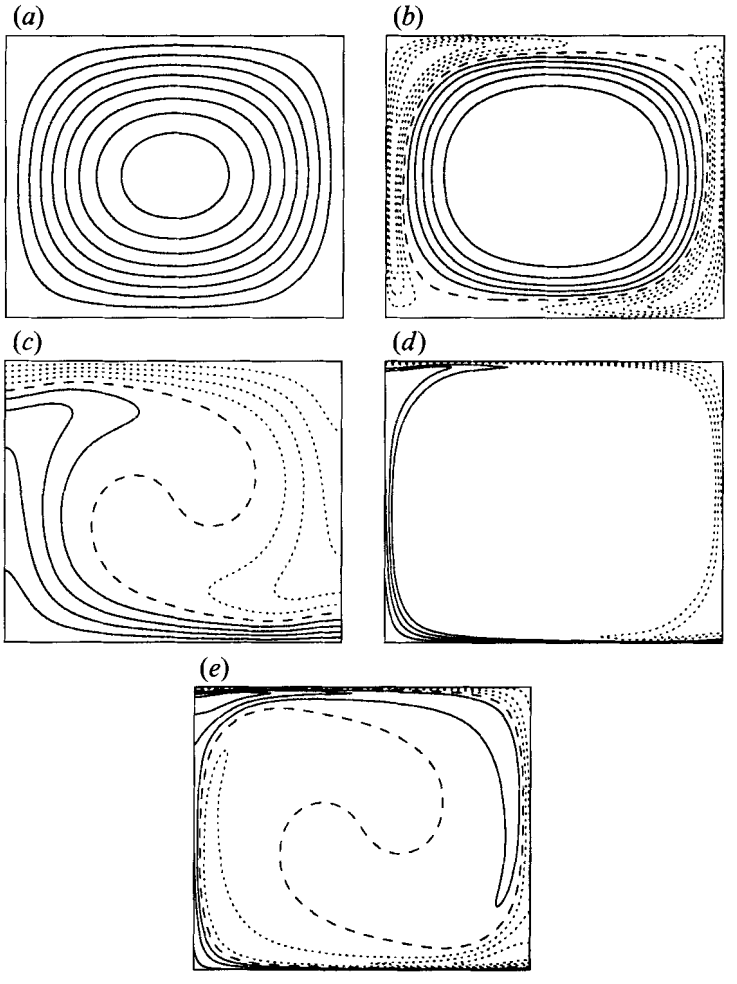

FIGURE 6. Contour plots of (*a*) Ψ, (*b*) ω, (*c*) T, (*d*) S and (*e*) ρ, for $R_a = 18305$, $R_s = 50305$, $\tau = 0.015$, $\sigma = 0.1$. Positive (negative) contours are shown as solid (dotted); the zero contour is dashed.

A similar result can be obtained from energy considerations, if $\tau^{1/2}R_s \gg 1$ (Proctor 1981). In the alternative limit, when $\tau^{-1/2} \gg R_s \gg 1$, Proctor found that

$$R_a^{min} \approx s^6/l^2 + \text{const} \times (\tau^2 R_s^4)^{1/7}. \tag{5.5}$$

We are only interested in the regime where $\tau \ll 1$ and $\tau^{1/2}R_s \gg 1$. From the numerical results contained in table 2 we find that $R_a^{min} \approx 2.3\tau^{1/2}R_s$ and thus, by comparison with equation (4.13), we see that the degree of subcriticality is indeed reduced from that predicted by the truncated model of §4, by a factor of $O(\tau^{1/2})$. On translating the thermosolutal result into magnetic buoyancy we obtain

$$R_t^{min} \approx \left[2.3\tau^{1/2} - \frac{\gamma - 1}{\gamma}\right] R_b \tag{5.6}$$

$$\approx -\frac{\gamma - 1}{\gamma} R_b \quad \text{for} \quad \tau^{1/2} \ll 1. \tag{5.7}$$

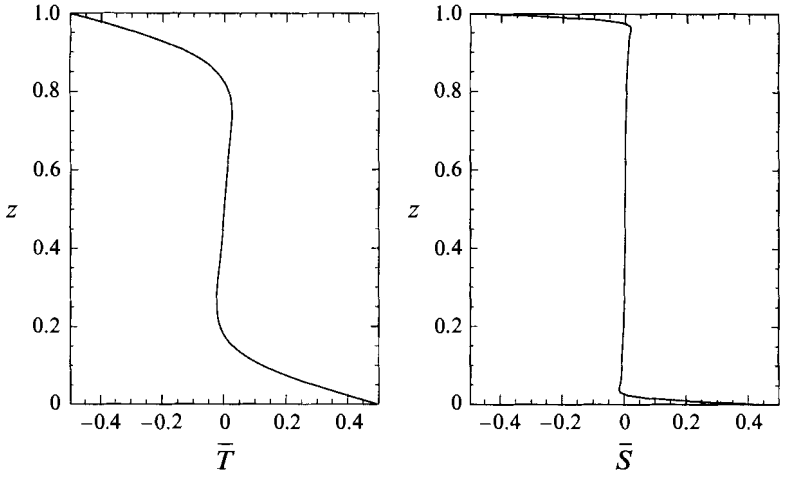

FIGURE 7. Horizontally averaged T and S versus height, for the solution shown in figure 6.

τ	R_t	R_a	R_s	N_a	N_s
0.015	−2000	18305	50305	4.54	34.53
0.04	5000	25833	50833	5.17	24.79
0.1	11000	33222	52222	4.85	14.59

TABLE 3. Turning-point values at a fixed value of R_b ($R_b = 50000$), $\sigma = 0.1$ and for three different values of τ. R_t is decreased in steps of 1000 until no steady solution is found.

It can be seen that expression (5.7) is identical with (4.17) for $\tau \ll 1$ and $R_b \gg 1$, and thus for the magnetic buoyancy problem, in this limit, the predictions of R_t^{min} from both the fifth-order system and the full equations are the same; the $\tau^{1/2}$ contribution in (5.6) becomes insignificant after translation into the (R_b, R_t)-plane. With our numerical simulations we are certainly not in the parameter regime where (5.7) is valid and so, as already pointed out, R_t^{min} considerably exceeds the prediction of the fifth-order system. From (5.6) we see that R_t^{min} can only be negative for $\tau^{1/2} \lesssim (\gamma - 1)/2.3\gamma$ or $\tau \lesssim 0.03$; with our value of $\tau = 0.015$ we are comfortably in the required regime, although both terms in (5.6) are still of comparable magnitude.

Our results confirm the linear dependence of R_t^{min} on R_b (cf. Huppert & Moore 1976). However, verifying numerically the τ dependence of R_t^{min} is difficult. Expression (5.6) is derived on the assumption that $\tau^{1/2} \ll 1$ and it is simply not feasible to conduct a series of numerical experiments for a range of τ satisfying this inequality. We have therefore just calculated the turning point values for $R_b = 50000$ with $\tau = 0.015$, 0.04 and 0.1; the results are contained in table 3. Using the results for our smallest value of τ ($\tau = 0.015$) we may amend (5.6) to give the more specific expression

$$R_t^{min} \approx 4500 + \left(2.3\tau^{1/2} - \frac{(\gamma - 1)}{\gamma}\right) R_b . \tag{5.8}$$

In figure 8, where the abscissa is $\ln \tau$, the dashed line depicts the function $\ln(2.3R_b) + 0.5 \ln \tau$; the three points marked with crosses are the three values of $\ln(R_t^{min} - 4500 + (\gamma - 1)R_b/\gamma)$ obtained from the simulations. We see that the agreement is reasonable for $\tau \leqslant 0.04$; it is, not surprisingly, rather poor for the larger value of $\tau = 0.1$, where the region of subcritical convection is somewhat greater than predicted by (5.8).

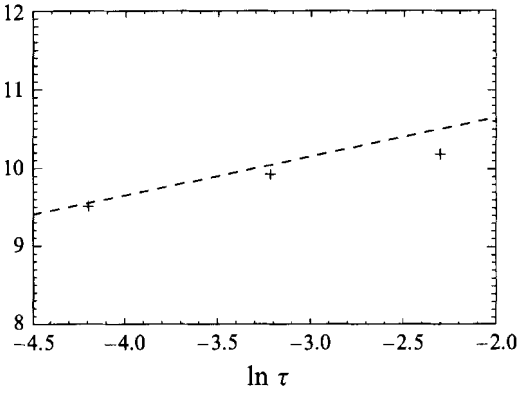

FIGURE 8. Comparison of the predictions of expression (5.8) with the results from the full PDEs. The abscissa is $\ln\tau$; the dashed line depicts the function $\ln(2.3R_b) + 0.5\ln\tau$, and the crosses are the values of $\ln(R_t^{min} - 4500 + (\gamma - 1)R_b/\gamma)$ obtained from the simulations for $\tau = 0.015$, 0.04 and 0.1 ($\sigma = 0.1$, $\gamma = 5/3$).

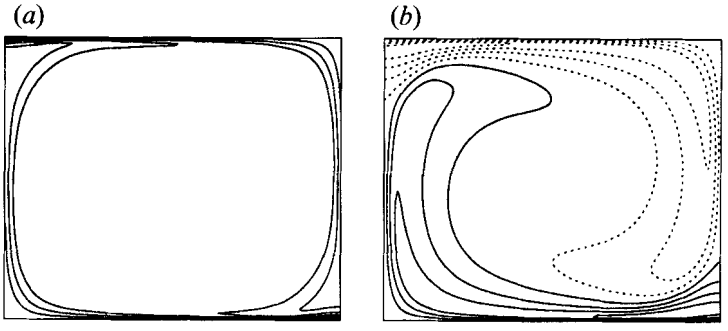

FIGURE 9. Contour plots of (*a*) χ_b (B/ρ) and (*b*) χ_p $(p\rho^{-\gamma})$ for the same solution as shown in figure 6 ($R_t = -2000$, $R_b = 50\,000$).

5.2. *The physical explanation*

Subcritical thermosolutal convection with $R_a > 0$, $R_s > 0$ and τ small is relatively straightforward to understand. However, when the results are formally translated to describe convection driven by magnetic buoyancy, implying steady convection with $R_t < 0$ and $R_b > 0$, they become distinctly counter-intuitive. It is therefore absolutely essential that we provide a convincing physical explanation of this phenomenon.

Figure 9 shows the contour plots of χ_b (B/ρ) and χ_p $(p\rho^{-\gamma})$, calculated using (2.19) and (2.20). The distribution of B/ρ is essentially that of S whereas the contours of $p\rho^{-\gamma}$ are more complicated, arising from a linear combination of those of T and S. Figure 10 plots the profiles of the horizontal averages of B/ρ and $p\rho^{-\gamma}$ and it is these that shed the most light on what is happening. Obviously, via equation (2.19), the distribution with depth of $\overline{B/\rho}$ is that of $\overline{S}$; it is the more complicated profile of $\overline{p\rho^{-\gamma}}$ (given by (2.20)), with its double boundary layer structure, that reveals the source of the unusual behaviour under investigation.

The magnetic pressure δp_m is concentrated into very thin boundary layers in which δp_m increases sharply with height. For thermosolutal convection, the boundary layer in temperature is $O(\tau^{-1/2})$ thicker than that in solute; using the relation (2.12) we can see that, for small τ, the thermal boundary layers for both thermosolutal convection and magnetic buoyancy are of comparable thickness. In the Boussinesq approximation,

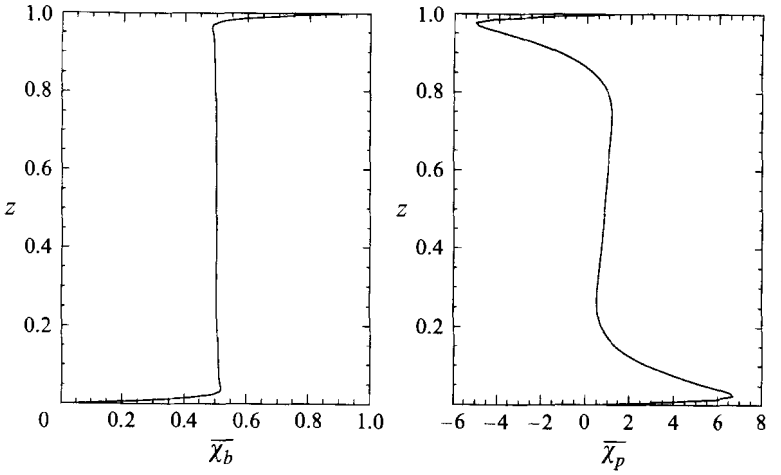

FIGURE 10. Horizontally averaged χ_b and χ_p as functions of height, for the solution shown in figure 9.

variations in total pressure are small (i.e. $\delta p \approx -\delta p_m$); thus in the magnetic boundary layer we have the following balance:

$$\frac{1}{p_0}\frac{\mathrm{d}}{\mathrm{d}z}\delta p \approx \frac{1}{\rho_0}\frac{\mathrm{d}}{\mathrm{d}z}\delta\rho, \tag{5.9}$$

since $\mathrm{d}(\delta T)/\mathrm{d}z$ is small, and hence

$$\begin{aligned}\frac{1}{p_0}\frac{\mathrm{d}}{\mathrm{d}z}\delta p - \frac{\gamma}{\rho_0}\frac{\mathrm{d}}{\mathrm{d}z}\delta\rho &\approx \frac{1-\gamma}{p_0}\frac{\mathrm{d}}{\mathrm{d}z}\delta p \\ &\approx \frac{\gamma-1}{p_0}\frac{\mathrm{d}}{\mathrm{d}z}\delta p_m. \end{aligned}\tag{5.10}$$

In the magnetic boundary layers therefore, there is a large gradient in $p\rho^{-\gamma}$. In fact, the thin outer boundary layers in $p\rho^{-\gamma}$ are seen to be so exceptionally stable ($\mathrm{d}(p\rho^{-\gamma})/\mathrm{d}z$ large) that the value of $p\rho^{-\gamma}$ at the inner edge of the lower (upper) outer boundary layer 'overshoots' its value at the upper (lower) surface. To compensate, there is of necessity a negative (destabilizing) entropy gradient across the remainder of the cell; this is such as to drive steady convection, with a characteristic profile of $\overline{p\rho^{-\gamma}}$. Figure 10 shows clearly the dramatic extent of the distortion of the $p\rho^{-\gamma}$ profile. In the static state $\mathrm{d}\chi_p/\mathrm{d}z = \gamma$ ($\chi_p = 0$ at $z = 0$, $\chi_p = \gamma$ at $z = 1$); in the final steady convective state the range of χ_p is approximately 12 – i.e. 7 times the static variation. Thus, to sum up, we see that steady motion with two stabilizing gradients is made possible through the influence of the magnetic field on the convective stratification; this is dramatically different from thermosolutal convection, in which strong concentrations of solute in thin boundary layers do not have a profound effect on the temperature distribution.

6. Conclusion

We have investigated in detail nonlinear convection driven by magnetic buoyancy, for the case when the gradients of both B/ρ and $p\rho^{-\gamma}$ are, in the absence of diffusion, stabilizing. Our method of attack has been to study classical double-diffusive convection (thermosolutal convection) and then to relate the results to magnetic

buoyancy via the transformation of Spiegel & Weiss (1982). The truncated fifth-order system of §4 suggests the counter-intuitive possibility of steady convection in the stable–stable regime, but cannot give quantitative results concerning the extent of the subcritical behaviour. By high-resolution numerical simulations of the full governing partial differential equations we have however confirmed that this strange behaviour really does occur; equally importantly we have provided a physical explanation as to *why* it occurs. The key feature is the formation of narrow magnetic boundary layers which influence the convective stratification so as to make these layers extremely stable; as compensation there results a superadiabatic gradient across the bulk of the cell, and it is this that drives the steady convection.

Although these steady solutions are stable to point-symmetric disturbances that satisfy the boundary conditions (2.7), it is not obvious what will happen when those restrictions are relaxed. In Appendix B we describe nonlinear results obtained with periodic lateral boundary conditions, which require a different numerical code. We find that the same physical processes still operate, and that vigorous convection can still be found in the regime where both gradients are stable, although steady solutions give way to travelling waves. Thus we conclude that the mechanism is robust.

We have considered only two-dimensional flows, with all variables dependent only on x and z; the fluid motions take place in the (x, z)-plane and the magnetic field is in the y-direction. This geometry then allows us to combine the studies of thermosolutal convection and magnetic buoyancy via the transformation of Spiegel & Weiss. However, there is no reason why the strange behaviour that we have identified should be peculiar to this two-dimensional geometry. Having identified the underlying physical mechanism, we can see that steady convection with two stabilizing gradients should also occur for general three-dimensional flows (though in this case there is no formal analogy with thermosolutal convection). Similarly, although the presence of horizontal boundaries is of course an essential feature, we do not regard our specific choice of boundary conditions as being of fundamental importance in causing the unusual behaviour. For instance, we would still expect to find the same effect if the vertical gradients of Ψ and Θ, rather than their actual values, were set to zero in (2.7*a*), though the influence of the boundary layers might be less profound.

It is interesting to note that in addition to the analogy exploited throughout this paper, that between thermosolutal convection and magnetic buoyancy, there is a similar formal relationship between thermosolutal convection and convection in binary fluids (Knobloch 1980). We plan to see how the strange behaviour we have unearthed for magnetic buoyancy relates to that system.

Our primary motivation for studying magnetic buoyancy instabilities is to improve our understanding of the solar magnetic field. Observations of the surface magnetic field (see, for example, Stix 1989) imply that the Sun's interior field is predominantly azimuthal; furthermore, theoretical studies suggest that the field resides mainly in the convective overshoot zone, a thin mildly subadiabatic region ($R_t < 0$) sandwiched between the radiative zone below and the convection zone above. The field is maintained against dissipation by dynamo action; on occasion, it escapes and rises to the surface where it erupts to form magnetic active regions and sunspots. The distribution of magnetic field through the overshoot zone, and its escape into the convection zone, are regulated by magnetic buoyancy instabilities. It is well-known that magnetic fields tend to be unstable if B/ρ decreases upwards; what we have established is that finite-amplitude instability can occur if B/ρ increases with height. Thus any variation is likely to promote magnetic buoyancy instabilities.

The key feature behind the unusual phenomenon of steady convection with two stabilizing gradients is the formation of narrow magnetic boundary layers and their influence on the convective stratification. In the Sun the boundary conditions are, of course, less clear cut than in our idealized model. Nonetheless, horizontal boundaries of a kind do exist; the lower boundary condition on the field comes from an abrupt increase with depth in the subadiabatic gradient, the upper boundary of the field is determined by the nature of the magnetic flux expulsion from the turbulent convection zone above. There is thus potential for the formation of magnetic boundary layers and, if B/ρ increases upwards ($R_b > 0$), for steady convection of the type we have been discussing. The effect of such convection would be to modulate the distribution of the field with depth by preventing the field gradient exceeding a threshold value. Almost certainly though, instabilities driven by two stabilizing gradients are not the whole story. For example, instabilities of the salt-fingering type are possible if B/ρ decreases with height ($R_t < 0$, $R_b < 0$). Indeed, where the magnetic field decreases sharply at the upper boundary of the overshoot zone there is potential for an extreme version of such an instability, with magnetic gas supporting less dense non-magnetic gas (a magnetic Rayleigh–Taylor instability). The nonlinear evolution of this instability has been studied both in two dimensions (Cattaneo & Hughes 1988; Cattaneo, Chiueh & Hughes 1990) and, very recently, in three dimensions (Matthews, Hughes & Proctor 1995). The latter calculation, in particular, seems capable of explaining certain features of the formation of magnetic active regions. A full theory must of course account not only for the whole range of possible magnetic buoyancy instabilities but also for the generation of the field by dynamo action.

We are very grateful to Dr D.R. Moore for providing us with the computer code used to obtain the results of §5, and for subsequent numerical advice. We should also like to thank Dr M.R.E. Proctor and Professor J. Toomre for helpful discussions on double-diffusive convection. This work was supported in part by NASA through grants NSG-7511, NAGW-91 and NAG5-513, by the SERC (and its successor PPARC), by the Nuffield Foundation and by Trinity College, Cambridge.

Appendix A. Derivation of (2.19) and (2.20)

For descriptive purposes it is natural to choose the fields B/ρ and $p\rho^{-\gamma}$, since it is the gradients of these quantities that are responsible for driving convection driven by magnetic buoyancy (see equation (1.4)). Furthermore, this description is the most economical, involving just the Rayleigh numbers and the diffusivity ratios σ, τ. If, for example, we wished to calculate the distribution of B (rather than B/ρ) then it would be necessary to specify, in addition, the initial stratification of B.

First, decompose B and ρ into sums of their equilibrium and perturbation components:

$$B = B_0(1 - \zeta z/d) + b, \qquad \rho = \rho_0(1 - \xi z/d) + \delta\rho. \tag{A 1}$$

Since, in the Boussinesq approximation, the layer depth d is assumed much smaller than all relevant scale heights, then $|\zeta|, |\xi| \ll 1$. Thus

$$\frac{B}{\rho} = \frac{B_0(1 - \zeta z/d + b/B_0)}{\rho_0(1 - \xi z/d + \delta\rho/\rho_0)} \approx \frac{B_0}{\rho_0}\left(1 - \frac{\zeta z}{d} + \frac{\xi z}{d} + \frac{b}{B_0} - \frac{\delta\rho}{\rho_0}\right). \tag{A 2}$$

The perturbation in the total pressure is assumed small; hence $\delta p \approx -\delta p_m$ and the

perfect gas law becomes

$$\frac{\delta\rho}{\rho_0} = -\frac{\delta T}{T_0} - \frac{\delta p_m}{p_0}, \tag{A 3}$$

all three terms being of comparable size. Thus comparing, in order of magnitude, the final two terms in expression (A2), we find that

$$\frac{\delta\rho/\rho_0}{b/B_0} \approx \frac{\delta\rho/\rho_0}{\delta p_m/(B_0^2/\mu_0)} \sim \frac{B_0^2/\mu_0}{p_0} = \frac{V_A^2}{V_S^2}, \tag{A 4}$$

where $V_A^2 = B_0^2/\mu_0\rho_0$ is the square of the Alfvén speed and $V_S^2 = p_0/\rho_0$ is the square of the isothermal sound speed. In the Boussinesq approximation the speed of sound is much greater than that of any other wave; hence $V_A^2 \ll V_S^2$ and $\delta\rho/\rho_0$ is negligible in comparison with b/B_0. Hence, from (A2),

$$\frac{B}{\rho} \approx \frac{B_0}{\rho_0}\left(1 + z\frac{\mathrm{d}}{\mathrm{d}z}\ln\left(\frac{B}{\rho}\right) + \frac{\delta p_m}{B_0^2/\mu_0}\right). \tag{A 5}$$

After a suitable rescaling we obtain the following dimensionless form for B/ρ:

$$B/\rho = \text{const.} + R_b(z - \Sigma). \tag{A 6}$$

Hence, to illustrate the variation in B/ρ, we choose to use the variable χ_b, defined by

$$\chi_b = \mathrm{sgn}(R_b)[z - \Sigma]. \tag{A 7}$$

In a similar fashion,

$$\frac{p}{\rho^\gamma} \approx \frac{p_0}{\rho_0^\gamma}\left(1 + z\frac{\mathrm{d}}{\mathrm{d}z}\ln\left(\frac{p}{\rho^\gamma}\right) + \frac{\delta p}{p_0} - \gamma\frac{\delta\rho}{\rho_0}\right) \tag{A 8}$$

$$\approx \frac{p_0}{\rho_0^\gamma}\left(1 + z\frac{\mathrm{d}}{\mathrm{d}z}\ln\left(\frac{p}{\rho^\gamma}\right) + (\gamma - 1)\frac{\delta p_m}{p_0} + \gamma\frac{\delta T}{T_0}\right). \tag{A 9}$$

After rescaling we obtain the following dimensionless expression:

$$\frac{p}{\rho^\gamma} = \text{const.} - \gamma R_t z + \left(\frac{1-\gamma}{1-\tau}\right)R_b\Sigma + \Theta\left(\gamma R_t + \frac{(\gamma-1)}{(1-\tau)}R_b\right). \tag{A 10}$$

Thus, to illustrate the variation in $p\rho^{-\gamma}$ we introduce the variable χ_p, defined by

$$\chi_p = (\mathrm{sgn}(R_t))\left(-\gamma z + \left(\frac{1-\gamma}{1-\tau}\right)\frac{R_b}{R_t}\Sigma + \Theta\left(\gamma + \frac{(\gamma-1)}{(1-\tau)}\frac{R_b}{R_t}\right)\right). \tag{A 11}$$

Appendix B. Changing the lateral boundary conditions

Our main aim in this paper has been to identify, and then to explain, the unusual behaviour that can arise in a system with stabilizing magnetic and entropy gradients. To achieve this end we have adopted the simplest possible configuration – two-dimensional motions with the impermeable lateral boundary conditions (2.7) and the imposition of point-symmetry. Nevertheless, it is of some interest to examine how the picture is changed by relaxing these constraints. In particular, we shall here consider the effects of simultaneously admitting solutions that lack point-symmetry and introducing periodic lateral boundary conditions, thereby allowing flow across the boundaries. Solving equations (2.3)–(2.5) then requires a completely different code and we are deeply grateful to Dr D.R. Moore for modifying his program to deal

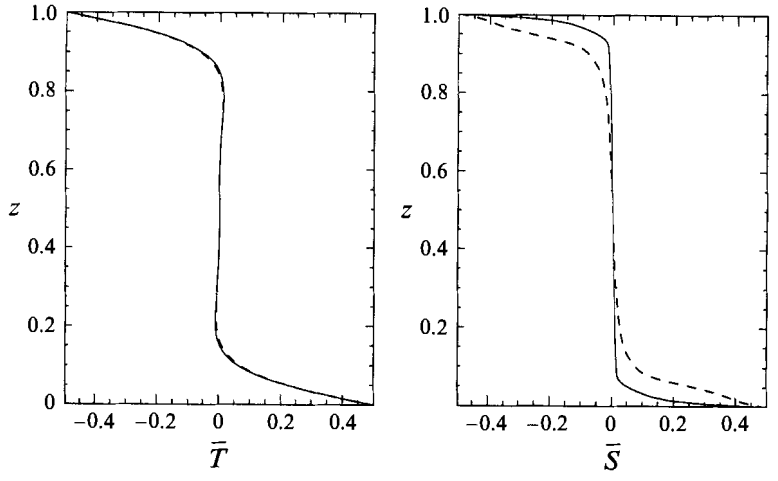

FIGURE 11. Horizontally averaged T and S versus height, for the modulated travelling wave solution with $R_a = 29\,457$, $R_s = 75\,457$ ($R_t = -1000$, $R_b = 75\,000$). The solid (dashed) lines are when N_s is maximized (minimized).

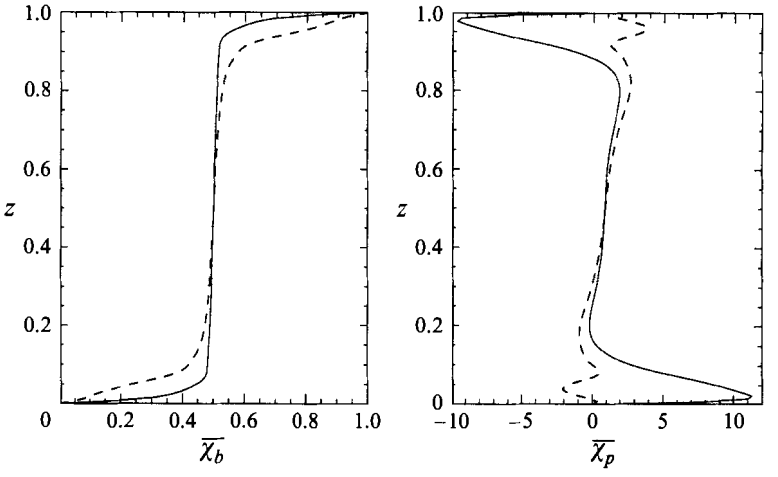

FIGURE 12. Horizontally averaged χ_b and χ_p as functions of height, for the solution shown in figure 11 ($R_t = -1000$, $R_b = 75\,000$).

with this more general configuration. This is now a fairly expensive computational task: for the same resolution, four times as much storage is needed with periodic boundary conditions as for symmetric solutions with boundary conditions (2.7) and we therefore need 384 × 128 grid points. Consequently we have not attempted to investigate large regions of parameter space; instead we have examined the solutions at a fixed value of R_b ($R_b = 75\,000$) and a few values of R_t.

For thermosolutal convection it is well-known that standing waves are unstable and travelling waves are stable near the initial Hopf bifurcation (Bretherton & Spiegel 1983; Knobloch *et al.* 1986). Moreover, the branch of travelling waves joins the upper portion of the steady branch well beyond the turning point, at $R_a = R_a^{TW}$, so that the steady solution is only stable for $R_a > R_a^{TW} > R_a^{min}$ (e.g. Moore & Weiss 1990). We find that the steady solutions in the convectively stable quadrant (with $R_t < 0$) are indeed unstable. Even when $R_t = 10\,000$ (convectively unstable) the preferred

solution is a travelling wave, propagating without change of form. As R_t is reduced, the travelling wave becomes modulated by an oscillation in the solutal (or magnetic) boundary layer. For $R_t = -1000$ (and hence in the interesting stable–stable quadrant) the solutal Nusselt number N_s varies between a maximum of 30.3 and a minimum of 7.9; there is much less variation in the thermal Nusselt number N_a, which oscillates between 6.47 and 6.15. (For the corresponding steady solution, which is now unstable, $N_s = 46.7$ and $N_a = 6.08$.) Figure 11 shows the horizontally averaged temperature and salinity distributions at those times when N_s is at its maximum and minimum. There is a marked variation in the thickness of the pulsating solutal boundary layers whereas any differences in the thermal boundary layers are too small to perceive. The corresponding profiles of B/ρ and $p\rho^{-\gamma}$ are shown in figure 12. The most interesting feature of the figure is that, when N_s is maximized, the influence of the magnetic boundary layer on the distribution of $p\rho^{-\gamma}$ is precisely the same as for the more restricted steady solutions discussed in detail above; i.e. extremely stable boundary layers are formed, with an unstable entropy gradient in the bulk of the cell. When N_s is small, and the solutal (magnetic) boundary layers are thick, there is relatively little variation in $p\rho^{-\gamma}$ with depth.

We may thus conclude that the unusual physical mechanism that we have identified is still of importance when the lateral boundary conditions are changed. With periodic boundary conditions, vigorous convection still takes place (in the form of modulated travelling waves) with the entropy gradient determined (at least during much of the oscillations) by the magnetic boundary layers.

REFERENCES

ACHESON, D. J. 1979 Instability by magnetic buoyancy. *Solar Phys.* **62**, 23–50.

BRETHERTON, C. & SPIEGEL, E. A. 1983 Intermittency through modulational instability. *Phys. Lett.* A **140**, 152–156.

CATTANEO, F., CHIUEH, T. & HUGHES, D. W. 1990 Buoyancy-driven instabilities and the nonlinear breakup of a magnetic layer. *J. Fluid Mech.* **219**, 1–23.

CATTANEO, F. & HUGHES, D. W. 1988 The nonlinear breakup of a magnetic layer: instability to interchange modes. *J. Fluid Mech.* **196**, 323–344.

CORFIELD, C. N. 1984 The magneto-Boussinesq approximation by scale analysis. *Geophys. Astrophys. Fluid Dyn.* **29**, 19–28.

DA COSTA, L. N., KNOBLOCH, E. & WEISS, N. O. 1981 Oscillations in double-diffusive convection. *J. Fluid Mech.* **109**, 25–43.

GALLOWAY, D. J., PROCTOR, M. R. E. & WEISS, N. O. 1978 Magnetic flux ropes and convection. *J. Fluid Mech.* **87**, 243–261.

HUGHES, D. W. 1985 Magnetic buoyancy instabilities for a static plane layer. *Geophys. Astrophys. Fluid Dyn.* **32**, 273–316.

HUGHES, D. W. 1992 The formation of flux tubes at the base of the convection zone. In *Sunspots: Theory and Observations* (ed. J. H. Thomas & N. O. Weiss), pp. 371–384. Kluwer.

HUGHES, D. W. & PROCTOR, M. R. E. 1988 Magnetic fields in the solar convection zone: magneto-convection and magnetic buoyancy. *Ann. Rev. Fluid Mech.* **20**, 187–223.

HUPPERT, H. E. & MOORE, D. R. 1976 Nonlinear double-diffusive convection. *J. Fluid Mech.* **78**, 821–854.

HUPPERT, H. E. & TURNER, J. S. 1981 Double-diffusive convection. *J. Fluid Mech.* **106**, 299–329.

KNOBLOCH, E. 1980 Convection in binary fluids. *Phys. Fluids* **23**, 1918–1920.

KNOBLOCH, E., DEANE, A. E., TOOMRE, J. & MOORE, D. R. 1986 Doubly diffusive waves. *Contemp. Maths* **56**, 203–216.

MATTHEWS, P. C., HUGHES, D. W. & PROCTOR, M. R. E. 1995 Magnetic buoyancy, vorticity and three-dimensional flux tube formation. *Astrophys. J.* **448**, 938–941.

MOORE, D. R. & WEISS, N. O. 1990 Dynamics of double convection. *Phil. Trans. R. Soc. Lond.* A **332**, 121–134.

MOORE, D. R. & WEISS, N. O. & WILKINS, J. M. 1991 Asymmetric oscillations in thermosolutal convection. *J. Fluid Mech.* **233**, 561–585.

PROCTOR, M. R. E. 1981 Steady subcritical thermohaline convection. *J. Fluid Mech.* **105**, 507–521.

SPIEGEL, E. A. & WEISS, N. O. 1982 Magnetic buoyancy and the Boussinesq approximation. *Geophys. Astrophys. Fluid Dyn.* **22**, 219–234.

STIX, M. 1989 *The Sun.* Springer-Verlag.

TURNER, J. S. 1973 *Buoyancy Effects in Fluids.* Cambridge University Press.

VERONIS, G. 1965 On finite amplitude instability in thermohaline convection. *J. Mar. Res.* **23**, 1–17.